

# Development of Pure Poly Vinyl Chloride (PVC) with Excellent 3D Printability and Macro- and Micro-Structural Properties

*Davood Rahmatabadi, Kianoosh Soltanmohammadi, Mohammad Aberoumand, Elyas Soleyman, Ismaeil Ghasemi, Majid Baniassadi, Karen Abrinia, Mahdi Bodaghi,\* and Mostafa Baghani\**

Unmodified polyvinyl chloride (PVC) has low thermal stability and high hardness. Therefore, using plasticizers as well as thermal stabilizers is inevitable, while it causes serious environmental and health issues. In this work, for the first time, pure food-grade PVC with potential biomedical applications is processed and 3D printed. Samples are successfully 3D printed using different printing parameters, including velocity, raster angle, nozzle diameter, and layer thickness, and their mechanical properties are investigated in compression, bending, and tension modes. Scanning electron microscopy is also used to evaluate the bonding and microstructure of the printed layers. Among the mentioned printing parameters, raster angle and printing velocity influence the mechanical properties significantly, whereas the layer thickness and nozzle diameter has a little effect. Images from scanning electron microscopy also reveal that printing velocity greatly affects the final part's quality regarding defective voids and rasters' bonding. The maximum tensile strength of 88.55 MPa is achieved, which implies the superiority of 3D-printed PVC mechanical properties compared to other commercial filaments. This study opens an avenue to additively manufacture PVC that is the second most-consumed polymer with cost-effective and high-strength features.

molds, considerable material waste, and heavy peripherals.<sup>[1–3]</sup> This technique is based on the deposition of 2D sliced layers on top of each other to create a 3D object.<sup>[4,5]</sup> The intrinsic latitude of the AM technique has brought unique practicality for manufacturing particular customized samples in the biomedical, automotive, aerospace, construction, and food industries. Fused Filament Fabrication (FFF) or Fused Deposition Modeling (FDM) technique as a subset of the material extrusion method is the most developed and promising technique for thermoplastics AM.<sup>[6,7]</sup> FDM method works on an easy basis of extruding semi-molten filament using G-code-driven movement to produce a part.<sup>[8–10]</sup> Several commercialized engineering thermoplastic filaments have developed as the FDM feedstock like PLA, ABS, HIPS, PETG, PA6, TPU, etc.<sup>[5,8,9,11–13]</sup> But, there are demands on a larger variety of consumable thermoplastic feedstock with a wider diversity of mechanical, optical, thermal, and intelligent properties,

to make FDM one of the most reliable thermoplastic manufacturing techniques.

Polyvinyl chloride (PVC) is a transparent and commonly amorphous thermoplastic.<sup>[14–16]</sup> Cost efficiency, excellent mechanical properties (stiffness and impact strength), chemical resistance,

## 1. Introduction

Additive manufacturing (AM) or 3D printing is a newly emerged fabrication method that can produce complex geometries without

D. Rahmatabadi, K. Soltanmohammadi, M. Aberoumand, E. Soleyman, M. Baniassadi, K. Abrinia, M. Baghani  
 School of Mechanical Engineering  
 College of Engineering  
 University of Tehran  
 Tehran 1417614411, Iran  
 E-mail: baghani@ut.ac.ir

I. Ghasemi  
 Faculty of Processing  
 Iran Polymer and Petrochemical Institute  
 Tehran 1497713115, Iran  
 M. Bodaghi  
 Department of Engineering  
 School of Science and Technology  
 Nottingham Trent University  
 Nottingham NG11 8NS, UK  
 E-mail: mahdi.bodaghi@ntu.ac.uk

© 2022 The Authors. Macromolecular Materials and Engineering published by Wiley-VCH GmbH. This is an open access article under the terms of the Creative Commons Attribution License, which permits use, distribution and reproduction in any medium, provided the original work is properly cited.

DOI: 10.1002/mame.202200568

and durability make PVC to be one of the most used commercial plastics in the world in the construction, electrical, automotive, medical, and packing industry.<sup>[14,16–18]</sup> PVC can be processed via most of the melt processing techniques, such as extrusion, injection, and blow molding regarding its high melt viscosity.<sup>[14]</sup> Pure PVC is plasticized mostly by the addition of phthalate esters (PAEs) up to 10% for the rigid form to 70% for the soft form, to provide a wide variety of flexibility.<sup>[16,19]</sup> However, PVC has some drawbacks as tremendous thermal degradation (yellowing) close to its processing temperature at 170 °C that can be extended to higher temperatures by the addition of thermal stabilizers.<sup>[14]</sup> Besides, migration of the phthalate esters plasticizers has been found to deteriorate the plasticization effect in addition to its hazardous danger, at least for childcare toys and food packing.<sup>[18,19]</sup> In general, additives, average molecular weight, and their distribution determine the final physical and chemical properties of a PVC product.<sup>[18]</sup>

Even though PVC is usually introduced as an amorphous polymer, there is a limited degree of crystallinity and ordered structure within the commercial PVC microstructure making its processing challenging.<sup>[20–22]</sup> Small Angle X-ray Scattering (SAXS) and Small Angle Neutron Scattering (SANS) data have also proved the existence of a poor crystalline network spacing of  $\approx 100$  nm.<sup>[22,23]</sup> These less-ordered and well-dispersed crystallites are connected by tie molecules, forming a network inside the PVC sample regarding the molecular weight (chain length). The higher *K* value (higher viscosity and molecular weight) of PVC leads to a more effective 3D network because the longer molecular chain can serve as tie molecules more efficiently.<sup>[24]</sup> Therefore, the crystallinity and the resultant molecular network of PVC make its rheological properties hard to compatible with extrusion-based AM. Thus, lots of variables should be considered for the 3D printing of PVC. To the best of the authors' knowledge, there are a few research works on the feasibility of PVC 3D printing. For instance, Calafel et al.<sup>[25]</sup> investigated suitable rheological conditions for FFF 3D printing of the plasticized PVC employing DINP from 10% up to 40 wt.% in which the final filament could be completely flexible. They failed to investigate the mechanical properties. Nevertheless, they concluded that higher nozzle diameters enhance printability with the aid of filament buckling prevention. More rigid filaments with higher compressive modulus withstand buckling employing lower nozzle diameter. Shear thinning of PVC makes its rheological behavior more suitable at higher shear rates (higher printing speeds) but higher volumetric output flow leads to buckling. PVC filament printability was examined at printing temperatures of 180 to 210 °C. Although no buckling occurred at lower printing temperatures, the existence of a tiny crystalline network causes clogging during extrusion. Thus, a higher temperature below its degradation point seems suitable for the 3D-printing of PVC. They also introduced self-plasticized PVC-acrylate copolymers as suitable PVC-based feedstock for 3D bio-printing.<sup>[26]</sup> Peñas et al.<sup>[27]</sup> introduced Phase-Separated PVC-Acrylate Copolymers that can be printed by screw-driven 3D printing but not FDM because of their high melt viscosity. Singh et al.<sup>[28]</sup> manufactured a biocompatible filament composed of 70% PVC, 30%PP, and 40% Hap for FDM 3D printing with applications in scaffold porous structures<sup>[29]</sup> and bio-sensing.<sup>[30]</sup> Lewenstam et al.<sup>[31]</sup> modified an FDM 3D printer to directly print a pre-fabricated composite block of highly

loaded PVC by KCL salt, employing a piston and extrusion die. Kumar et al.<sup>[32,33]</sup> prepared a magnetic composite of PLA-PVC-wood dust-Fe<sub>3</sub>O<sub>4</sub> for FDM 3D printing by addition of 25 wt.% of PVC just to improve the flowability of the composite.

Limited operating temperature range, poor adhesion between rasters, high melt strength, and buckling are issues with PVC 3D printing by FDM. The extraordinary plasticization strategy was utilized to address this issue in all previous cases, which deteriorates the superior mechanical properties of rigid PVC by making the final product flexible as an elastomer. Although small molecule plasticizers such as phthalate esters increase the toughness and improve the rheological properties of PVC, their migration phenomenon affects the modified PVC's long-term performance and causes health problems.

Therefore, in this research, for the first time, food-grade pure PVC has been successfully additively manufactured by controlling and adjusting printing parameters. It has both the advantages of not overusing destructive and unsanitary additives and obtaining the most superior macro-structural mechanical properties among the FDM printed samples with other commercial filaments. The nozzle printing temperature of 200 °C was selected as the main parameter while raster angle, layer thickness, printing velocity, and nozzle diameter were also determined as variable parameters to investigate the mechanical properties. The macro-structural mechanical properties studies include tensile, flexural, and compressive tests, as well as Scanning Electron Microscopy (SEM) imaging. Finally, to elaborate on the importance of using PVC in 3D printing, the results of tensile mechanical properties were compared with available 3D-printed thermoplastics. The results of this research, as a comprehensive experimental work, can attract attention to employing PVC for AM and expand the diverse applications of PVC 3D printing.

## 2. Experimental Section

### 2.1. Materials and 3D Printing

Nontoxic food-grade PVC granules prepared by Pishro Plast Bepar Co. with a *K* value of 65 were selected as the raw material. The *K* value provides important information about the physical properties (mechanical and rheological) of PVC's molecular weight, its distribution, and the related viscosity. Skillicorn et al.<sup>[34]</sup> reported that the PVC with a *K* value of 65 has an inherent viscosity of 0.88 dL g<sup>-1</sup>,  $M_n = 38.5 \times 10^3$  g mol<sup>-1</sup>,  $M_w = 78.0 \times 10^3$ , and PDI  $\approx 2$ .

To print the final samples by FDM, first, a filament with a diameter of 1.75 mm along with smooth surface was developed using a laboratory-made single-screw extruder equipped with a 1.75 mm diameter circular die, with a length over diameter ratio of 15 and stage temperature of 210 °C. The shear rate of the extruder was set at 25 rpm using a servo-motor. After qualitative and quantitative examination of PVC filaments, the printing of samples began using a laboratory-made single nozzle FDM 3D printer. For the first time, several vital points were considered to print the samples due to the special conditions of PVC printing. Because of the PVC's poor adhesion on the printer's bed, PVC pipe glue was used to ensure the adhesion of the first layer. The most important challenge in PVC printing is the choice of printing temperature. As mentioned before, there is a very

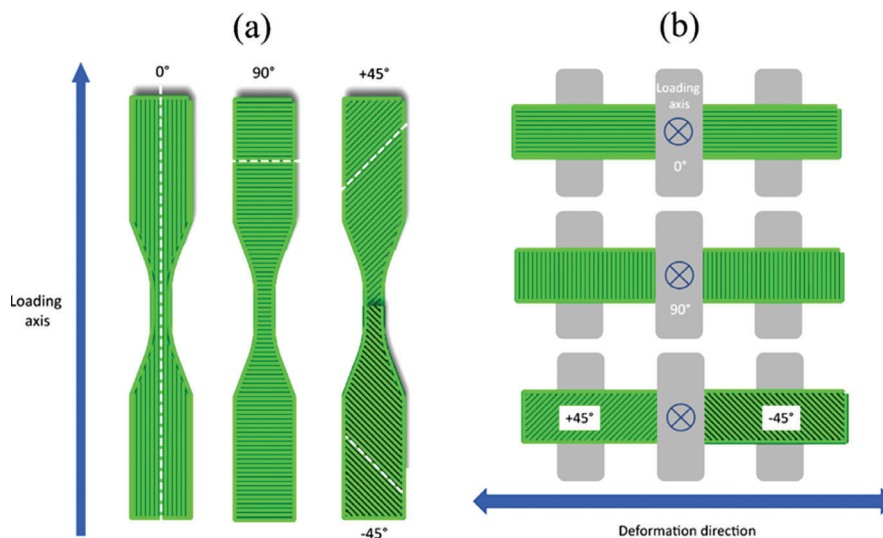


**Figure 1.** Definition of RA relative to loading and/or deformation direction for a) tensile and b) flexural tests.

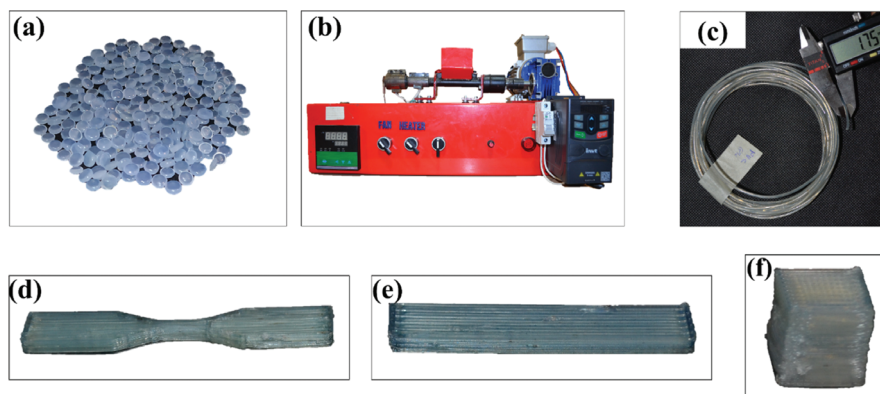


**Figure 2.** Materials and equipment used: a) PVC granules, b) extruder, c) PVC filaments, printed samples of d) tensile, e) bending, and f) compression tests.

limited operating temperature range whose cooperation with other printing parameters such as speed, nozzle diameter, and layer thickness affects the rheological behavior, bucking and quality of the manufactured parts. For this purpose, the constant nozzle printing temperature of 200 °C was considered for all samples, and to achieve the optimal mechanical properties, printing speed, layer thickness, and nozzle diameter were manipulated considering printability. It should be noted that this temperature was the highest possible one for PVC printing and any increment could cause thermal degradation (yellowing). The color change and yellowing of some printed samples according to **Figure 1** are also due to this issue. Of course, it is possible to print at lower temperatures (range 180–200 °C) under certain printing conditions and parameters. However, lowering the printing temperature causes incomplete melting of PVC crystals and higher melt strength, which manifests itself in different ways during printing. They are listed as nozzle clogging, filament buckling, and poor deposition.

All the samples were prepared with 100% infill density at the platform temperature of 60 °C. Variable parameters are presented in **Table 1**. Figure 1 shows the definition of the Raster An-

**Table 1.** Selected PVC printing parameters range to investigate the effect of Raster Angle (RA), Velocity (V), Nozzle Diameter (ND), and Layer Thickness (LT) on mechanical properties.

	Sample	ND [mm]	LT [ $\mu\text{m}$ ]	V [ $\text{mm s}^{-1}$ ]	RA (°)
<b>Effect of RA</b>	1	0.8	200	20	0
	2	0.8	200	20	90
	3	0.8	200	20	$\pm 45$
<b>Effect of V</b>	4	0.8	200	30	0
	1	0.8	200	20	0
<b>Effect of ND</b>	5	0.8	200	10	0
	1	0.8	200	20	0
<b>Effect of LT</b>	6	0.4	200	20	0
	5	0.8	200	10	0
	7	0.8	300	10	0

gel (RA) relative to the loading or/and deformation axis for two tensile and flexural tests. Also, equipment, materials, and printed samples for mechanical tests are presented in **Figure 2**.

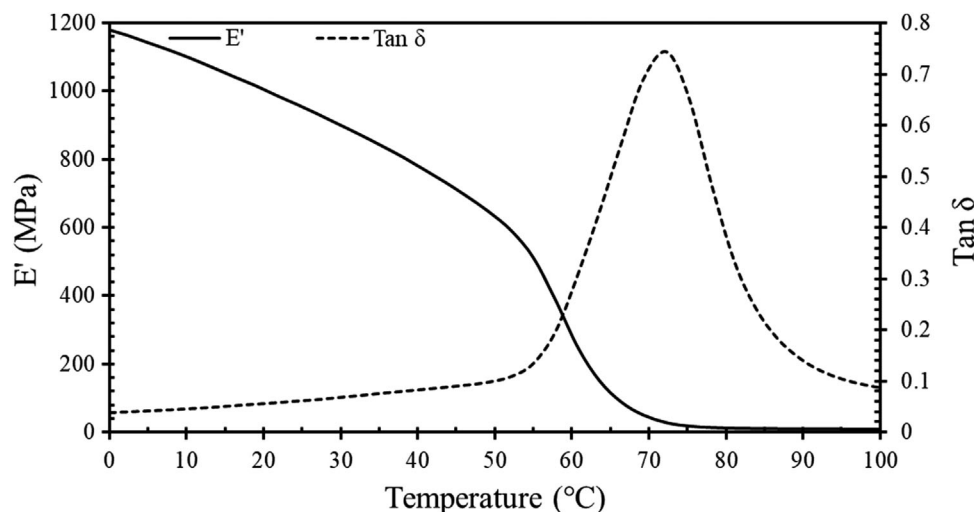


Figure 3. DMTA curve of the 3D printed PVC sample.

## 2.2. DMTA and SEM

Dynamic mechanical thermal analysis (DMTA) test was performed to investigate the thermomechanical behavior and to determine the different thermal zones of PVC. This test was conducted by a dynamic mechanical thermal analyzer (Mettler Toledo, Switzerland) over a temperature range from  $-20$  to  $120$  °C with a  $5$  °C  $\text{min}^{-1}$  heating rate and a constant  $1$  Hz frequency using a cantilever 3D printed beam with the geometry of  $40 \times 10 \times 1$  mm under bending mode (ASTM D4065-01 standard).

Imaging was also performed using the SEM to evaluate the bonding quality between layers. Before imaging, the samples were immersed in liquid nitrogen and then coated with gold. Imaging was performed using PhilipsXL30 Scanning Electron Microscope (The Netherlands) with secondary electron imaging mode.

## 2.3. Mechanical Properties

Uniaxial tensile, compression, and flexural tests were performed on all seven groups of PVC samples presented in Table 1 to investigate the macro-structural mechanical properties and the effect of printing parameters. All the samples were successfully printed except for the compression test sample for group 4. Compression samples have smaller dimensions ( $10 \times 10 \times 10$  mm) than the bending and tension tests, and the printing time of each layer is much shorter. With an increase in velocity ( $30$  mm  $\text{s}^{-1}$ ), this time becomes shorter, and the movement of the nozzle on the uncooled layer causes the surface to get deteriorated. Therefore, the bottom molten layer cannot support the next printing layer, bringing about a lack of inter-layer adhesion. Tensile specimens were printed according to the ASTM D638 type V standards. Due to the validity of the tensile test results, five samples were prepared for each sample code. After checking the results, the data with a difference of  $>20\%$  compared to the average were removed, and then the average and standard deviation

using the STDEV.S function in Excel software were calculated and reported for each parameter. The compression test standard was ISO604:2002 that was used by Ratiu et al.<sup>[35]</sup>. A flexural test was conducted on samples printed in the dimensions of  $50 \times 10 \times 3$  mm using a three-point bending fixture equipped with cylindrical supports with a diameter of  $5$  mm and center to center distance of  $30$  mm. All the tests were performed, at a displacement rate of  $3$  mm  $\text{min}^{-1}$ , at room temperature. A universal testing machine manufactured by Khallagh Sanat Atieh Peyman Company equipped with an S-shaped load cell with an accuracy of  $0.1$  N was employed for testing.

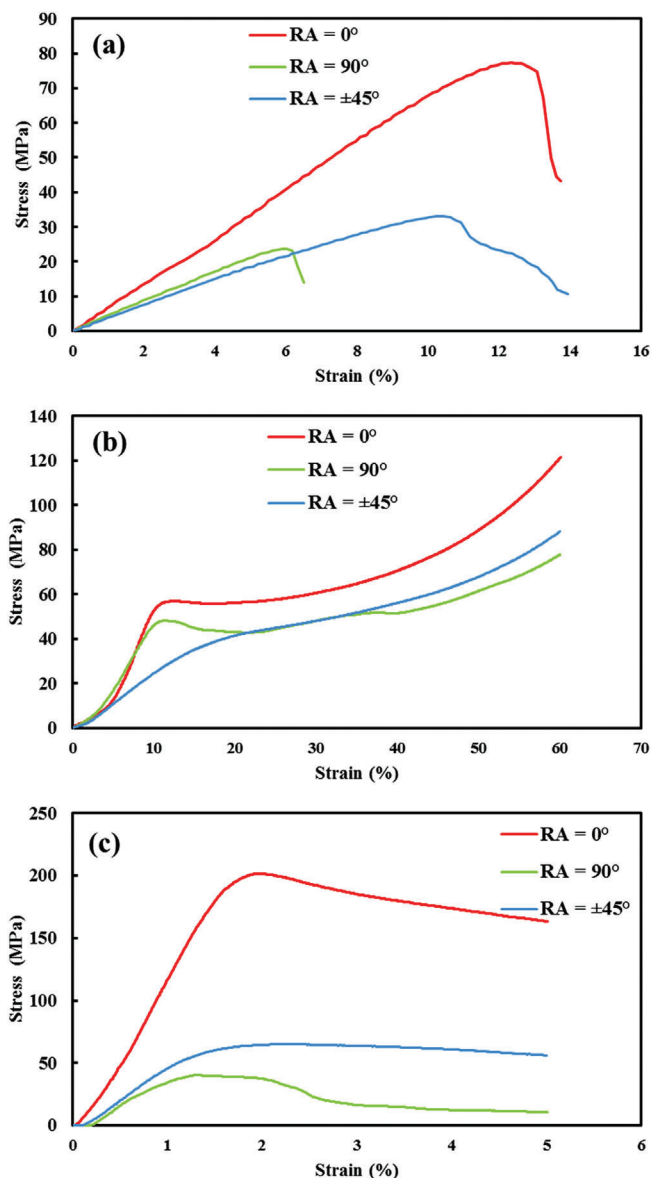
## 3. Results and Discussion

### 3.1. DMTA

Figure 3 demonstrates the DMTA result of the 3D-printed PVC sample. Tan  $\delta$  peak represents the glass-to-rubber transition, which ranges from  $55$  to  $85$  °C with a central peak of  $72$  °C as the glass transition temperature ( $T_g$ ). The storage modulus shows a constant decrease with an increase in temperature before showing a steep decrease  $\approx 55$  °C, as the start of the glass-to-rubber transition. According to the available literature, the addition of essential additives to the PVC, like thermal stabilizer, fire retardant, and plasticizer results in a continuous decrease in the storage modulus with increasing the temperature that can also be seen in Figure 3.<sup>[25,36]</sup> It makes the modified rigid PVC product exhibit a vast range of stiffness before the main glass-to-rubber transition.

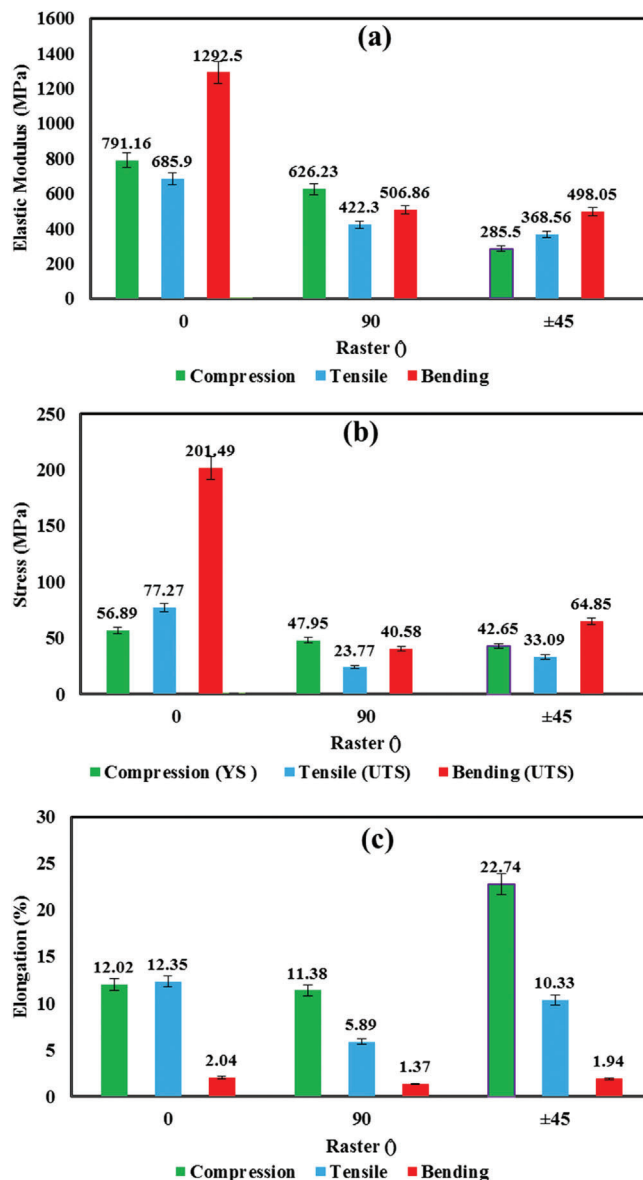
### 3.2. Effect of Raster Angle

Figure 4 shows the results of uniaxial tensile, compression, and flexural tests (stress-strain curves) for investigating the effect of different RAs on mechanical behaviors. Also, the quantitative results extracted from Figure 4 are presented in Figure 5 for



**Figure 4.** Effect of raster angle on the mechanical behavior of PVC 3D printed with FDM under a) tensile, b) compression, and c) bending modes.

various mechanical parameter examinations. According to Figure 4, RA is a basic controlling printing parameter that can be altered to achieve the desired mechanical properties. The effect of RA on mechanical behavior such as strength, elongation, and elastic modulus under different loading modes is well observed due to the orientation-dependent nature of mechanical properties.<sup>[37,38]</sup> The best properties are obtained for the sample with the RA in the same direction as the loading axis. The maximum effect of the RA has appeared in the tensile and flexural modes. The bending deformation mode also has a tensile nature of the longitudinal tension and compression in the top and bottom region of the neutral axis, respectively, making the tensile and bending behaviors have a relatively same trend as the RA alteration.<sup>[39]</sup> The maximum tensile and flexural strengths are



**Figure 5.** Results of tensile, compression, and bending tests for different raster angles.

77.27 and 201.49 MPa, respectively, for the sample with RA of 0, while for the sample with RA of 90, these values fall to 23.77 and 40.58 MPa, respectively. This considerable difference (3.25 and 4.97 times for tensile and bending modes) is due to the failure mechanism and the rupture start point. Sample 3 exhibits lower deformation stress with an almost same failure strain and broader and gentler post UTS stress drop than sample 1. It can be deduced that sample 3 has a softer behavior than sample 1. The lack of a distinct detectable yield point for sample 3 in both compression and flexural tests can be introduced as another characteristic of the softer failure. According to the literature, two types of failure mechanisms, including failure in the raster and debonding or open linkage in the fibers, are dominant in printed PVC samples as well as other printed thermoplastics such as PLA and ABS.<sup>[40–42]</sup> For sample 1 with the RA in the same direction as

the loading axis, the rupture in the rasters causes the failure. In fact, the rasters are stretched in the applied force direction and their tearing causes failure in the sample. In contrast, for sample 2 with the RA of 90, the applied force is concentrated at the raster interfaces, which are the weakest areas of FDM 3D printed parts due to the presence of cracks and defects that resulted from incomplete raster coalescence. Therefore, these factors cause a de-bonding failure mechanism associated with a sharp drop in the results of the tensile properties leading to the lowest amount of the obtained mechanical properties for RA of 90. For the altered RA of  $\pm 45$ , the failure mechanism is slightly different. As a matter of fact, the strength and elongation are determined according to the percentage and changing the angle of the accompanying rasters. Therefore, the sample with an RA of  $\pm 45$  has lower and greater strength than samples 1 and 2, respectively. Also, the highest amount of elongation (12.35%) was obtained for sample 1. In fact, in sample 3, the rotation of the PVC rasters in the tension direction delays the rupture and prevents sudden and brittle failure, and increases the elongation. Thus, the elongation for sample 3 (10.33%) with  $\pm 45$  RA is more than sample 2 that is consistent with previous research.<sup>[39,43]</sup>

Figure 4b shows the uniaxial compression tests of samples 1–3. Samples 1 and 3 show distinctive yield stress and a subsequent stress-hardening. The yield stress of samples 1 and 3 is 62.29 and 46.45 MPa, respectively. Because of the out-of-plane mode selection for the compression test, samples 1 and 2 have the same raster angle relative to the loading direction. The nature of compression makes the interlayer voids and cracks get close in out-of-plane loading.<sup>[44]</sup> As a result, there is no detectable macroscopic rupture regarding Figure 4b. On the other hand, the possibility of stress concentration at the interface of the adjacent rasters due to printed layers expansion in out-of-plane compression may have acted as the most destructive phenomenon. These two competitive phenomena may result in an increase or decrease in yield stress and elastic modulus by the dominance of each. The compression-induced crack closure causes samples to exhibit a detectable yield, and subsequent strain-hardening occurs rather than sudden rupture without any particular yield point of the tensile test. The lower compressive yield stress of sample 1 than its tensile mode may result from a more concentrated yield at the raster's interface (as weaker zones for stress concentration) in each layer. Also, the higher compressive elastic modulus may stem from the mentioned crack closure. Despite the tensile test, out-of-plane compression may justify the lower compression modulus of sample 3 than its tensile modulus because of the absence of the raster rotation in sample 3. On the other hand, opposite to the tensile test, the lack of direct perpendicular deformation on the interface of adjacent rasters in the compression test may have increased the compression yield stress of sample 3. Figure 4c shows the results of the bending test for different RAs that are consistent with the results of Figure 4a for the tensile test. It may result from the same deformation nature of the tensile of the bending test and it is consistent with the reference.<sup>[37]</sup> The significant differences between tensile and bending results can be summarized as the lower strain at maximum stress in bending as well as its higher maximum stress. There is an excess intralayer shear stress development in bending while half of the sample thickness is under compression and a similar phenomenon was observed in reference.<sup>[45]</sup> These men-

tioned significant differences between tensile and flexural deformation modes cause higher strength with more brittle behavior in bending than tension. These dissimilarities between tensile and bending have also been observed and reported in the literature, see, e.g., Refs.<sup>[46,47]</sup>. The most important defect in the 3D printed parts is the high density of cavities, which its effects become less visible. Also, the intralayer welding effect should be considered in the case of intralayer shear stress development.

### 3.3. Effect of Velocity

The stress–strain diagrams of tensile, compression, and flexural tests for 3D printed PVC samples printed with three different velocities of 10, 20, and 30 mm s<sup>-1</sup> are shown in **Figures 6** and **7**. As in the previous section, the most remarkable different effects of printing velocity are observed in the tensile and flexural tests since the resultant defects play a more pronounced role in these loading modes compared to the compression. The tensile strength ranges between 57.05 and 88.55 MPa for the three samples, while it is between 60.29 to 66.7 MPa for compression mode. According to Figure 6, sample 5 that is printed with the velocity of 10 mm s<sup>-1</sup>, has the best mechanical properties in all the loading modes. Generally, the lower printing speeds of 10 and 20 mm s<sup>-1</sup> exhibit the most negligible influence, while it gets harsher for printing speeds of 30 mm s<sup>-1</sup> for all loading modes to some extent. The major phenomenon followed by printing temperature alteration is the deposited molten rasters' temperature and the related melt elasticity, well-affecting porosity size, as well as rasters' interfacial strength. The lower printing velocity causes more completed melting of the filament, resulting in lower viscosity and higher extrudate temperature. This circumstance can cause better bonding or even fusion between layers and neighbor rasters, respectively.<sup>[48]</sup> Thus, the printing speed of 30 mm s<sup>-1</sup> seems to be the critical speed that significantly affects the 3D printed part strength. By raising the velocity, the trend decreases such that it is not possible to print the compression sample at the velocity of 30 mm s<sup>-1</sup>. Also, according to Figure 6c, samples with the velocity of 10 and 20 mm s<sup>-1</sup> have almost similar properties, which may be contributed to the simple non-curved geometry of bending samples. So, it can be said that another determinative factor in choosing the velocity of 3D printing of PVC samples is the geometry complexity.

### 3.4. Effect of Nozzle Diameter and Layer Thickness

The effects of nozzle diameter (0.4 and 0.8 mm) on the mechanical properties of the 3D printed PVC samples in tension, compression, and bending are shown in Figure 6. Utilizing a lower nozzle diameter needs a higher pressure for extruding the filament (see Ref. <sup>[25]</sup> for more details). To address this issue, viscosity modification by increasing the printing temperature seems to be the only option. The possibility of PVC-burning makes a limitation on printing temperature increase due to the nozzle clogging. Therefore, ND of 0.4 mm as a minimum suitable diameter for investigation has been selected with the same printing temperature of 0.8 mm nozzle. It is also recommended to use a smaller nozzle diameter to achieve a more desirable and better dimensional accuracy and surface roughness, which results

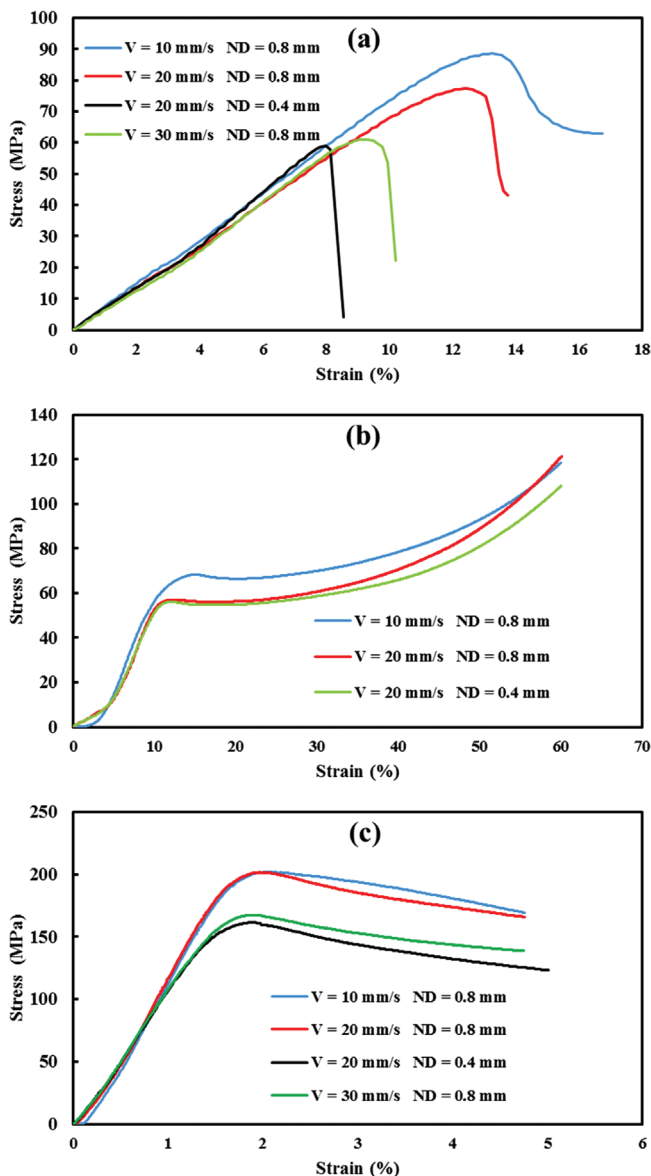


**Figure 6.** Effect of velocity and nozzle diameter on the mechanical behavior of PVC 3D printed with FDM under a) tensile, b) compression, and c) bending modes.

in an unsuitable increase in the printing time, at least for large structures. According to Figure 6b, the nozzle diameter does not significantly affect the mechanical properties in the compression mode. The two curves with different nozzle diameters are perfectly matched until the post-yield strain of 30%. The results of mechanical properties illustrated in Figure 7 reveal that by increasing the nozzle diameter from 0.4 to 0.8 mm, the yield stress and the elastic modulus in compression mode change by 0.2% and 2.41%, respectively. This ineffectiveness of ND is also observed in Figure 6a,c in the linear region, indicating the same elastic modulus in tensile and flexural loading modes. Moreover, in Figure 6a, the tensile strength for the sample 3D printed using a 0.8 mm diameter nozzle is greater. Employing a nozzle with a higher diameter with the same layer thickness causes the output

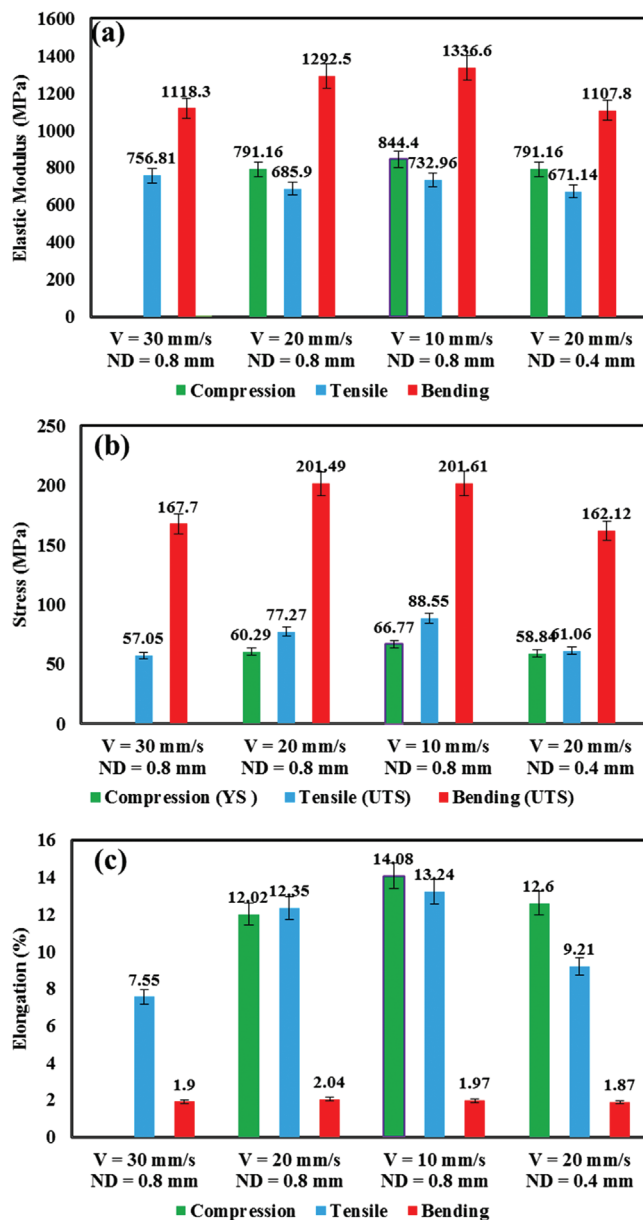


**Figure 7.** Results of tensile, compression, and bending tests for different printing velocities and nozzle diameters.

extrudate cross-section geometry to be more elliptical, making the resultant voids smaller. Ghorbani et al. investigated the effect of melt extrusion rate on mechanical properties, especially the geometry of cracks, and showed that with an increase in extrusion rate, the geometry changes and their size decreases, while they can be removed with a further increase in the extrusion rate.<sup>[49]</sup> In addition, higher demanded pressure for extruding through a narrower nozzle may be affected by the limitation of the rotating extruder's gears-induced pressure without the subsequent filament slippage. This may result in underfeeding and intensifying defect formation. All phenomena mentioned earlier cause a substantial drop in mechanical behavior by considerable defects formation and lack of sufficient interfacial contacts for samples 3D printed with a 0.4 mm diameter nozzle.

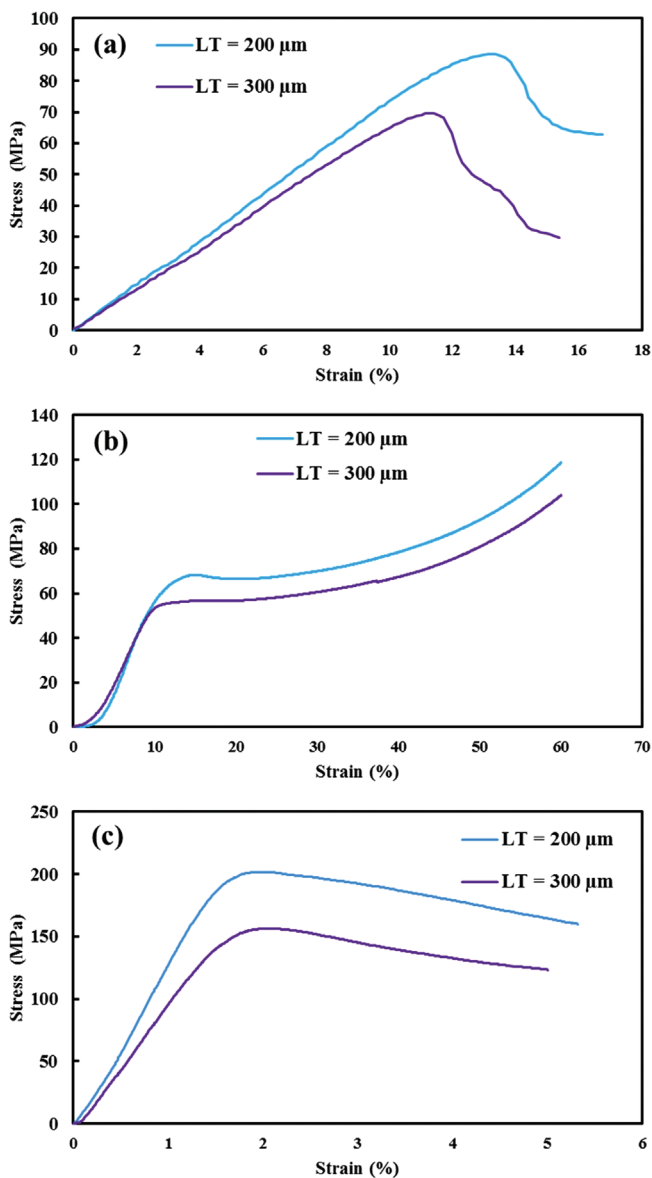


**Figure 8.** Effect of layer thickness on the mechanical behavior under a) tensile, b) compression, and c) bending modes.

**Figure 8** demonstrates the effect of layer thickness (200 and 300  $\mu\text{m}$ ) on mechanical properties. The same trend is observed in all three loading modes. It is also found that the layer thickness of 200  $\mu\text{m}$  has a significant advantage in mechanical properties. According to **Figure 9**, the yield stress, tensile and flexural strength for the 200  $\mu\text{m}$  layer thickness are, respectively, 1.16, 1.27, and 1.28 times higher than those with the 300  $\mu\text{m}$  layer thickness. These trends for PEEK,<sup>[50]</sup> ABS,<sup>[51]</sup> and PLA<sup>[52,53]</sup> have been approved by previous researchers.

### 3.5. SEM

**Figure 10** exhibits the failure cross-section images of 3D-printed PVC specimens printed with different printing parameters by

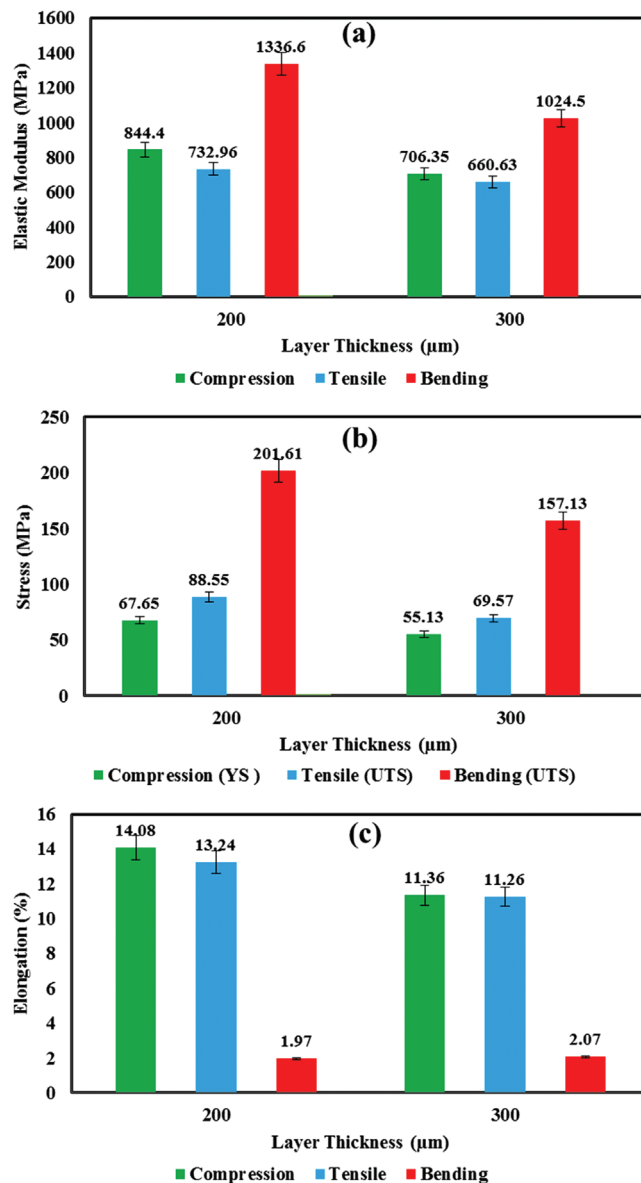


**Figure 9.** Results of tensile, compression, and bending tests for different layer thicknesses.

material extrusion. As can be seen, all samples have voids between the adjacent rasters as well as intralayer ones and this issue is unavoidable in 3D-printed parts by FDM. According to the figures, these voids were formed during FDM printing in intra and interlayer rasters. Internal voids can result from incomplete neck growth between adjacent intra and interlayer rasters.<sup>[54–56]</sup> In fact, ideally, the rasters should be completely merged, which is not possible because the rasters cool down very quickly and complete integration (crack growth) does not take place.<sup>[57]</sup> Therefore, these cavities are present in all samples due to the rapid cooling rate, incomplete melting, and differences in the thermal properties of the two successive layers. Furthermore, the amount, number, geometry, and size of these voids can be controlled by adjusting some printing parameters. Among the most important

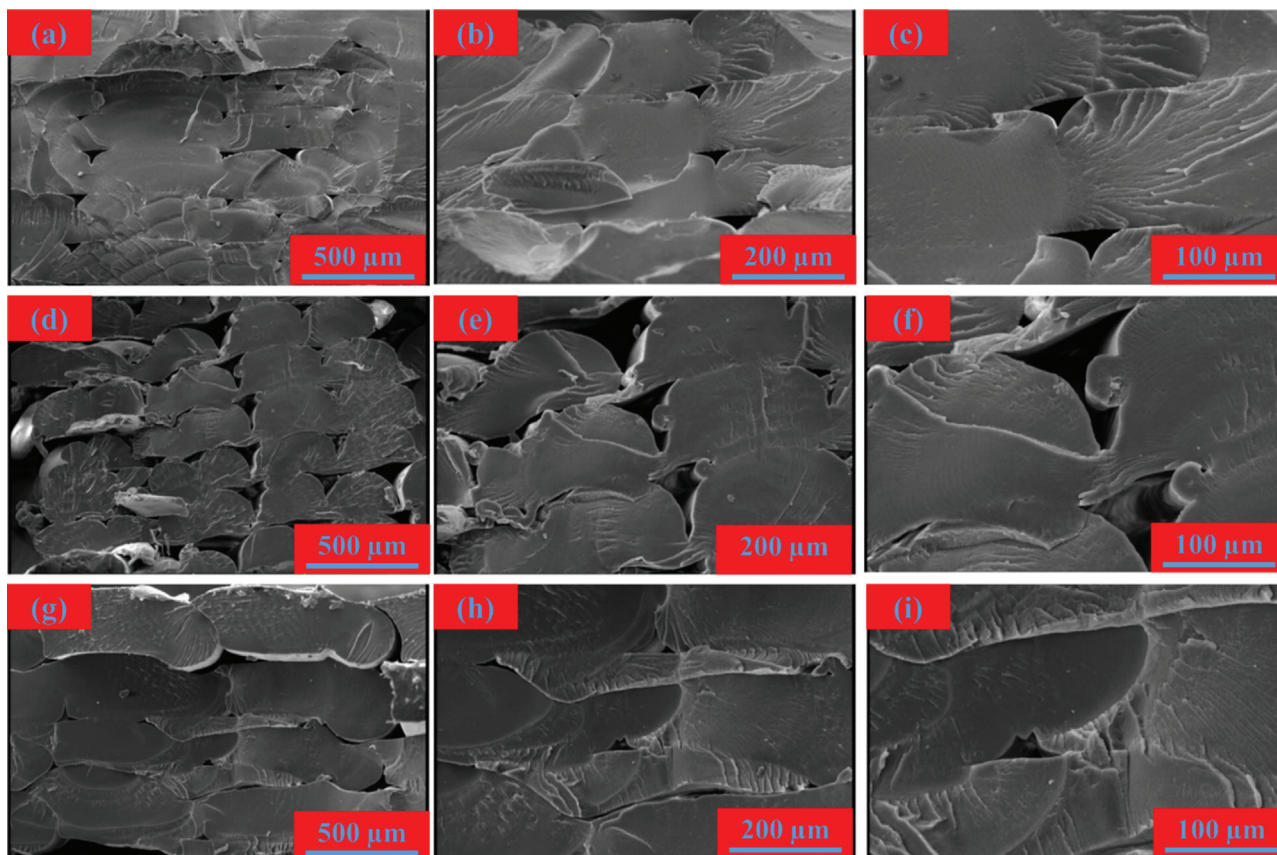


**Figure 10.** SME images for the failure cross-section of printed PVC specimens with different printing parameters: a–c)  $V = 10 \text{ mm s}^{-1}$ ,  $ND = 0.8 \text{ mm}$ , and  $LT = 200 \mu\text{m}$ , d–f)  $V = 20 \text{ mm s}^{-1}$ ,  $ND = 0.4 \text{ mm}$ , and  $LT = 200 \mu\text{m}$ , and g–i)  $V = 10 \text{ mm s}$ ,  $ND = 0.8 \text{ mm}$ , and  $LT = 300 \mu\text{m}$ .

parameters, melt strength, rheology, feeding rate, and its system can be pointed out. Melt strength depends on raw material and temperature. Rheology is also controlled by a combination of velocity, temperature, and nozzle diameter parameters.<sup>[49,56]</sup> PVC is printed at the constant temperature of  $200 \text{ }^\circ\text{C}$  due to high melt strength and limitations in high-temperature printing (burning due to not using additives harmful to health and medicine) and this factor increases the possibility of buckling during printing. For this reason, using a lower velocity improves the melt flow and feeding process and the results of the mechanical properties also confirm this. For this reason, the two groups that have the biggest difference in rheology are selected for this evaluation (lower speed and larger nozzle diameter and vice versa). Figure 10a–c is associated with the sample with  $200 \mu\text{m}$  layer thickness,  $10 \text{ mm s}^{-1}$  printing velocity, and the nozzle diameter of  $0.8 \text{ mm}$ . The lowest printing speed of  $10 \text{ mm s}^{-1}$  has improved the melting procedure and the deposition of the extruded material due to the higher temperature of the molten filament, reducing the probability of the defect forming. On the other hand, the second sample (d–f) does not have an appropriate layer quality. Figure 10d–f depicts the cross-section of the sample with doubled printing velocity and halved nozzle diameter. The low quality of this group is due to high velocity (less opportunity to reduce melt strength), and smaller nozzle diameter (reduction of feeding rate). As discussed earlier, the cross-section geometry of the deposited rasters determines the contact interface with sur-

rounding rasters. Bigger cylindrical cross-section geometry leads to a smaller interface, while a more elliptical cross-section can result in the highest possible interface. The cross-section of the deposited filament through a wider nozzle with the same layer thickness is more elliptical than that of a narrower nozzle. Furthermore, the effects of the mentioned underfeeding due to the employing of a  $0.4 \text{ mm}$  nozzle are considerable. As shown in Figure 10d–f, the resultant voids are too large and in higher numbers. Besides, more completed interfaces have been formed between adjacent rasters by comparing the SEM images on the first and second rows of Figure 10. As mentioned, in the FDM process, the output volumetric flow and the extrudate's rheological condition, determining the final product's quality, are controlled using a combination of printing parameters such as nozzle temperature, velocity, nozzle diameter, and layer thickness. Comparing Figure 10g–i with (a–c) reveals that the layer thickness increases by 50%, while the other printing parameters are kept constant. As can be seen, the average size and portion of the porosities for the sample with a higher layer thickness seem to be higher because of the cross-sectional geometry of the rasters. Hernandez et al. used an experimental-modeling approach to investigate the effect of layer thickness on the mechanical properties. They simulated the cross-section of printed rasters as two half-disks and a rectangle. Their results showed that increasing the layer thickness increased the density of the void ( $\approx$ decreased structural density) and reduced the tensile strength.<sup>[58]</sup> Also, printing with

**Table 2.** Effect of 3D printing parameters on the mechanical properties of PVC.

	Code	Compression		Tensile			Bending	
		E [mpa]	Ys [mpa]	E [mpa]	S [mpa]	El [%]	E [mpa]	S [mpa]
Effect of RA	1	791.16	60.29	685.90	77.27	12.35	1292.50	201.49
	2	626.23	51.32	422.30	23.77	5.89	506.86	40.58
	3	285.50	46.45	368.56	33.09	10.33	498.05	64.85
Effect of V	4	*	*	756.81	57.05	7.55	1118.3	167.70
	1	791.16	60.29	685.90	77.27	12.35	1292.50	201.49
Effect of ND	5	844.40	66.77	732.96	88.55	13.24	1336.6	201.61
	1	791.16	60.29	685.90	77.27	12.35	1292.50	201.49
Effect of LT	6	810.27	60.172	671.14	61.06	9.21	1107.8	162.12
	5	844.40	66.77	732.96	88.55	13.24	1336.6	201.61
	7	706.35	57.70	660.63	69.57	11.26	1024.5	157.13

higher layer thickness demands a higher output flow, leading to a lower temperature of the deposited filament with higher melt elasticity. This phenomenon results in a lack of complete diffusion and coalescence of adjacent rasters as well as intralayer. The poor interfaces act as a valuable site for crack propagation that is responsible for failure as reported in Ref.<sup>[59]</sup>.

### 3.6. Comparison of Mechanical Properties Results with Previous Research

The effect of printing parameters on the macro-structural mechanical properties of 3D-printed PVC samples is summarized in Table 2. As can be found, among the examined printing parameters, velocity, and raster angle play the most important roles, while layer thickness and nozzle diameter have the least impact. However, RA is determinative in all three loading modes; e.g., in the tensile and flexural, the difference in mechanical properties is very considerable. About the effect of velocity, under the same conditions, increasing printing speed from 10 to 20 mm s<sup>-1</sup> causes the tensile strength and elongation to decrease by 12.7% and 6.8%, respectively. In addition, the effect of printing parameters varies in different loading modes because the defects and void portion are more determinative in tensile and flexural tests than in compression. Sample 5, which is printed with a velocity of 10 mm s<sup>-1</sup>, raster angle 0, has the best mechanical properties among all samples. Compared to the worst sample (2), this model has the superiority of 3.77 and 4.98 times higher strength in tensile and flexural strength, respectively. Table 3 compares the tensile strength of 3D printed PVC with the tensile strength of other commercial 3Dprinting filaments reported in previous research works. As can be seen, the FDM feedstock collection clearly suffers from the absence of a high-strength material like PVC for FDM 3D printing technology. One of the main challenges in 3D printing with FDM is the low strength of the produced samples, getting most of the research in this field to focus on it. However, the proposed solutions for the use of new materials, post-heat treatment, and fabrication of different composites (use of fibers and nanoparticles) have produced new challenges. According to Table 3, the highest tensile strength achieved with PVC is 88.55 MPa, which is at least twofold greater than that of all

**Table 3.** Comparison of mechanical properties of the present 3D-printed PVC with other 3D-printed materials reported in the literature.

Material	Input	UTS	Reference
PVC	LT, V, ND, RA	88.55	This study
ABS	ID, LT, RA	33.78	[60]
ABS	IP, ID, LT	31.6	[61]
ABS	RA, RW, O	34.07	[62]
PETG	IP, LT, ID	30.25	[63]
PLA	IP	15.4	[64]
PLA	T, V, ID	45.27	[65]
PLA	LT, V, T, ND	45.82	[66]
Nylon	ID, V, LT	43.50	[67]
PEEK	ND, T, LT	73	[68]
PEEK	ND, V	74.24	[69]
PEEK	T, LT	77	[50]

conventional and commercial thermoplastics used in FDM such as ABS, PLA, PETG, and Nylon. It is a significant accomplishment compared to other samples made of other materials in previous studies. In addition, the mechanical properties obtained for PVC are even better than PEEK. Using PEEK is one of the solutions for printing high-strength parts, which comes with a much higher cost than other commercial filaments. The high price of the raw material, the need for additional equipment, a higher erosion rate, and more expensive printers due to the high printing temperature for PEEK are some of the limitations can be found this material. Therefore, the use of PVC can be one of the best options to solve the problems with the low strength of the FDM 3D printed part without an additional cost.

## 4. Conclusion

In the present research, for the first time, food-grade, non-modified PVC filament was processed and 3D printed by adjusting FDM 3D printing parameters. In fact, in this research, without overusing *f* destructive and unsanitary additives such as phthalate esters plasticizer, which is the first option to increase

the processability of PVC, tensile, pressure, and bending test samples were successfully printed. The effects of velocity, nozzle diameter, layer thickness, and raster angle were comprehensively investigated, and the following outstanding results were achieved:

- (a) A wide range of mechanical properties was obtained under the effect of printing parameters alteration as 23.77–88.55, 46.45–66.77, and 40.58–201.61 MPa for tensile, compression, and flexural strength, respectively. It shows the importance of FDM printing parameters, especially for PVC.
- (b) The effect of printing parameters on mechanical properties was greater in tensile and flexural loading modes. The difference between maximum and minimum tensile and flexural strengths was reported at 3.73 and 4.97, respectively, while this ratio was 1.44 in compressive mode. The most important defect in the 3D printed parts is the high density of cavities that are the source areas of crack growth and failure. Their closure in compression makes their effects less visible in comparison with tensile modes.
- (c) Raster angle and printing velocity had the greatest effect on the mechanical properties. Contrarily, the layer thickness and nozzle diameter exhibited the least effect. These results are consistent with previous research for other 3D printed materials. The RA changes the failure mechanism, while the velocity directly determines the output flow volume, temperature, and melt elasticity whereby the printing quality can change.
- (d) SEM results were consistent with mechanical properties. The velocity and layer thickness showed a significant effect on the cavities' density, their sizes as well as portions, and the fusion of the rasters.
- (e) The maximum amount of tensile strength for the PVC 3D printed samples was obtained in terms of 10 mm s<sup>-1</sup> printing velocity, 0.8 mm nozzle diameter, 200 μm layer thickness, and the raster angle of 0. Also, the highest tensile mechanical properties were obtained compared to other FDM commercial filaments, such as ABS, PLA, PETG, and PA.
- (f) The printing methodology in this research can be one of the simple and practical solutions to address the issue of the poor strength of PVCs 3D printed parts by FDM.

## Acknowledgements

In the original published version of this manuscript, M. Baniassadi was mistakenly listed as a corresponding author. This was corrected after on-line publication on December 13, 2022. The correct corresponding authors are M. Bodaghi and M. Baghani. The editorial office apologizes for any inconvenience caused.

## Conflict of Interest

The authors declare no conflict of interest.

## Keywords

3D printing, mechanical properties, polyvinyl chloride, printing parameters, SEM

Received: September 5, 2022  
Revised: November 7, 2022  
Published online:

- [1] N. Nguyen, J. G. Park, S. Zhang, R. Liang, *Adv. Eng. Mater.* **2018**, *20*, 1700876.
- [2] Y. Jiang, M. N. Islam, R. He, X. Huang, P. - F. Cao, R. C. Advincula, N. Dahotre, P. Dong, H. F. Wu, W. Choi, *Adv. Mater. Technol.* **2022**, 2200492. <https://doi.org/10.1002/ADMT.202200492>
- [3] J. Z. Manapat, Q. Chen, P. Ye, R. C. Advincula, *Macromol. Mater. Eng.* **2017**, *302*, 1600553.
- [4] A. Gebhardt, *Understanding Additive Manufacturing*, Carl Hanser Verlag GmbH & Co. KG, **2011**. <https://doi.org/10.3139/9783446431621>
- [5] T. D. Ngo, A. Kashani, G. Imbalzano, K. T. Q. Nguyen, D. Hui, *Compos. Part B Eng.* **2018**, *143*, 172.
- [6] O. A. Mohamed, S. H. Masood, J. L. Bhowmik, *Polym. Adv. Technol.* **2017**, *28*, 1911.
- [7] R. A. Wach, P. Wolszczak, *Macromol. Mater. Eng.* **2018**, *303*, 1800169.
- [8] A. Aminzadeh, M. Aberoumand, D. Rahmatabadi, M. Moradi, *Meta-heuristic Approaches for Modeling and Optimization of FDM Process*, **2021** 483–504. [https://doi.org/10.1007/978-3-030-68024-4\\_25](https://doi.org/10.1007/978-3-030-68024-4_25)
- [9] D. Rahmatabadi, A. Aminzadeh, M. Aberoumand, M. Moradi, in: *Fused Depos. Model. Based 3D Print*, Springer, Cham **2021**: pp. 131. [https://doi.org/10.1007/978-3-030-68024-4\\_7](https://doi.org/10.1007/978-3-030-68024-4_7)
- [10] M. Jin, R. Giesa, C. Neuber, H. W. Schmidt, *Macromol. Mater. Eng.* **2018**, *303*, 1800507.
- [11] B. N. Turner, R. Strong, S. A. Gold, *Rapid Prototyp. J.* **2014**, *20*, 192.
- [12] M. Aberoumand, K. Soltanmohammadi, E. Soleyman, D. Rahmatabadi, I. Ghasemi, M. Baniassadi, K. Abrinia, M. Baghani, *J. Mater. Res. Technol.* **2022**, *18*, 2552.
- [13] E. Soleyman, M. Aberoumand, D. Rahmatabadi, K. Soltanmohammadi, I. Ghasemi, M. Baniassadi, K. Abrinia, M. Baghani, *J. Mater. Res. Technol.* **2022**, *18*, 4201.
- [14] G. Akovali, *Toxic. Build. Mater.* **2012**, *23*. <https://doi.org/10.1016/B978-0-85709-122-2.50002-4>
- [15] A. Turner, M. Filella, *Environ. Sci. Process. Impacts.* **2021**, *23*, 1376.
- [16] B. Y. Peng, Z. Chen, J. Chen, H. Yu, X. Zhou, C. S. Criddle, W. M. Wu, Y. Zhang, *Environ. Int.* **2020**, *145*, 106106.
- [17] M. C. Sunny, P. Ramesh, K. E. George, *J. Elastomers Plastics* **2016**, *36*, 19. <http://doi.org/10.1177/0095244304038016>
- [18] S. Patrick, Rapra Technology Limited., *Practical guide to polyvinyl chloride*, **2005**, 162.
- [19] K. S. Carlos, L. S. de Jager, T. H. Begley, *Food Additives Contaminants: Part A* **2018**, *35*, 1214.
- [20] O. P. Obande, M. Gilbert, *J. Appl. Polym. Sci.* **1989**, *37*, 1713.
- [21] G. Pezzin, *Pure Appl. Chem.* **1971**, *26*, 241.
- [22] M. Gilbert, *J. Macromolecular Sci. Part C* **2006**, *34*, 77. <http://doi.org/10.1080/15321799408009633>
- [23] J. W. Summers, *J. Vinyl Technol.* **1981**, *3*, 107.
- [24] E. L. Hinrichsen, P. Thorsteinsen, *J. Vinyl Addit. Technol.* **1996**, *2*, 18.
- [25] I. Calafel, R. H. Aguirresarobe, M. I. Peñas, A. Santamaría, M. Tierno, J. I. Conde, B. Pascual, *Mater* **2020**, *13*, 178.
- [26] A. Santamaría, *eXPRESS Polymer Letters* **2018**, *12*, 824.
- [27] M. I. Peñas, M. I. Calafel, R. H. Aguirresarobe, M. Tierno, J. I. Conde, B. Pascual, A. Santamaría, *Polym* **2020**, *12*, 2070.
- [28] R. Singh, R. Sharma, J. P. Davim, *International Journal of Production Research* **2017**, *56*, 7330.
- [29] R. Sharma, R. Singh, R. Penna, F. Fraternali, *Compos. Part B Eng.* **2018**, *132*, 237.
- [30] R. Sharma, R. Singh, A. Batish, *Today Proc.* **2020**, *28*, 1115.

- [31] A. Lewenstam, B. Bartoszewicz, J. Migdalski, A. Kochan, *Electrochem. Commun.* **2019**, *109*, 106613.
- [32] S. Kumar, R. Singh, T. P. Singh, A. Batish, *Journal of Thermoplastic Composite Materials* **2019**, *34*, 929.
- [33] S. Kumar, R. Singh, T. P. Singh, A. Batish, *Journal of Thermoplastic Composite Materials* **2019**, *35*, 36.
- [34] D. E. Skillicorn, G. G. A. Perkins, A. Slark, J. V. Dawkins, *J. Vinyl Technol.* **1993**, *15*, 105.
- [35] M. Ratiu, M. A. Prichici, D. M. Anton, D. C. Negrau, *IOP Conf. Ser. Mater. Sci. Eng.* **2021**, *1169*, 012008.
- [36] K. Sałasińska, M. Barczewski, M. Celiński, P. Kozikowski, R. Kozera, A. Sodo, J. Mirowski, S. Zajchowski, J. Tomaszewska, *Polym* **2021**, *13*, 2909.
- [37] M. Dawoud, I. Taha, S. J. Ebeid, *J. Manuf. Process.* **2016**, *21*, 39.
- [38] I. I. Ailinei, S. V. Galatanu, L. Marsavina, *Mater. Des. Process. Commun.* **2021**, *3*. <https://doi.org/10.1002/MDP2.267>
- [39] J. Kiendl, C. Gao, *Compos. Part B Eng.* **2020**, *180*, 107562.
- [40] O. S. Es-Said, J. Foyos, R. Noorani, M. Mendelson, R. Marloth, B. A. Pregger, *Mater. Manuf. Process.* **2000**, *15*, 107.
- [41] R. Mendricky, D. Fris, *Teh. Vjesn.* **2020**, *27*, 1166.
- [42] S. H. Masood, K. Mau, W. Q. Song, *Mater. Sci. Forum* **2010**, *654-656*, 2556.
- [43] J. Santo, P. K. Penumakala, R. B. Adusumalli, *Polym. Compos.* **2021**, *42*, 3231.
- [44] F. He, V. K. Thakur, M. Khan, *Mater. Today Chem.* **2021**, *20*, 100393.
- [45] W. Riley, L. Sturges, D. Morris, *Flexural Loading: Beam Deflections, Mech. Mater.* 6th ed. **2006**.
- [46] I. Durgun, R. Ertan, *Rapid Prototyp. J.* **2014**, *20*, 228.
- [47] B. Akhoundi, A. H. Behraves, *Exp. Mech.* **2019**, *59*, 883.
- [48] T. C. Yang, C. H. Yeh, *Polym* **2020**, *12*, 1334.
- [49] J. Ghorbani, P. Koirala, Y. - L. Shen, M. Tehrani, *J. Manuf. Process.* **2022**, *80*, 651.
- [50] S. Xiaoyong, C. Liangcheng, M. Honglin, G. Peng, B. Zhanwei, L. Cheng, Experimental analysis of high temperature PEEK materials on 3D printing test, Proc. -9th Int. Conf. Meas. Technol. Mechatronics Autom. ICMTMA 2017. **2017** 13–16. <https://doi.org/10.1109/ICMTMA.2017.0012>.
- [51] A. K. Sood, R. K. Ohdar, S. S. Mahapatra, *Mater. Des.* **2010**, *31*, 287.
- [52] J. Torres, M. Cole, A. Owji, Z. DeMastry, A. P. Gordon, *Rapid Prototyp. J.* **2016**, *22*, 387.
- [53] J. M. Chacón, M. A. Caminero, E. García-Plaza, P. J. Núñez, *Mater. Des.* **2017**, *124*, 143.
- [54] P. K. Gurralla, S. P. Regalla, *Virtual and Physical Prototyping* **2014**, *9*, 141. <http://doi.org/10.1080/17452759.2014.913400>
- [55] J. E. Seppala, S. Hoon Han, K. E. Hillgartner, C. S. Davis, K. B. Migler, *Soft Matter* **2017**, *13*, 6761.
- [56] Y. Tao, F. Kong, Z. Li, J. Zhang, X. Zhao, Q. Yin, D. Xing, P. Li, *J. Mater. Res. Technol.* **2021**, *15*, 4860.
- [57] D. Bhalodi, K. Zalavadiya, P. K. Gurralla, *J. Brazilian Soc. Mech. Sci. Eng.* **2019**, *41*, 113.
- [58] S. Garzon-Hernandez, D. Garcia-Gonzalez, A. Jérusalem, A. Arias, *Mater. Des.* **2020**, *188*, 108414.
- [59] Q. Sun, G. M. Rizvi, C. T. Bellehumeur, P. Gu, *Rapid Prototyp. J.* **2008**, *14*, 72.
- [60] M. Samykan, G. Kanagaraj, S. K. Selvamani, K. Sudhakar, W. K. Ngui, K. Kadirgama, W. K. Ngui, G. Kanagaraj, K. Sudhakar, *Int. J. Adv. Manuf. Technol.* **2019**, *102*, 2779.
- [61] R. Srinivasan, T. Pridhar, L. S. Ramprasath, N. Sree Charan, W. Ruban, *Mater. Today Proc.* **2020**, *27*, 1827.
- [62] F. Rayegani, G. C. Onwubolu, *Int. J. Adv. Manuf. Technol.* **2014**, *73*, 509.
- [63] R. Srinivasan, W. Ruban, A. Deepanraj, R. Bhuvanesh, T. Bhuvanesh, *Mater. Today Proc.* **2020**, *27*, 1838.
- [64] M. Moradi, A. Aminzadeh, D. Rahmatabadi, A. Hakimi, *Mater. Res. Express.* **2021**, *8*, 035304.
- [65] S. Deshwal, A. Kumar, D. Chhabra, *CIRP J. Manuf. Sci. Technol.* **2020**, *31*, 189.
- [66] L. Yang, S. Li, Y. Li, M. Yang, Q. Yuan, L. Yang, S. Li, Y. Li, M. Yang, Q. Yuan, *J. Mater. Eng. Perform.* **2019**, *28*, 169.
- [67] M. Ramesh, K. Panneerselvam, *Mater. Today Proc.* **2021**, *46*, 9303.
- [68] P. Wang, B. Zou, H. Xiao, S. Ding, C. Huang, *J. Mater. Process. Technol.* **2019**, *271*, 62.
- [69] A. El Magri, K. El Mabrouk, S. Vaudreuil, H. Chibane, M. E. Touhami, *J. Appl. Polym. Sci.* **2020**, *137*, e49087.